Synthesis, Characterization, and Antibacterial Properties of a Hydroxyapatite Adhesive Block Copolymer

*Qiang Matthew Zhang, Michael J. Serpe **

Department of Chemistry, University of Alberta, Edmonton, AB, T6G 2G2

*Corresponding Author: Michael J. Serpe (michael.serpe@ualberta.ca)

Abstract

A novel diblock copolymer comprised of bisphosphonate and pyridine oligomers has been prepared by reversible addition-fragmentation transfer (RAFT) polymerization. Ag ion was introduced into the polymer via its coordination with the pyridine groups, followed by a reduction process to obtain Ag nanoparticles with diameters of 5-15 nm measured by transmission electron microscopy (TEM). In addition, x-ray photoelectron spectroscopy (XPS), and x-ray diffraction (XRD) proved successful introduction of Ag nanoparticles into polymer. Ag nanoparticles containing polymer exhibited excellent antibacterial properties toward Lactobacillus plantarum (*L. plantarum*). In order to investigate its practical application as antibacterial coating, the synthesized polymer was tethered onto hydroxyapatite (HA, main mineral component of natural bone, teeth, and most of implants for bone repair) surfaces via interaction between the polymer's bisphosphonate group and HA, forming ~4 nm thick layers. Ag nanoparticles (5-15 nm in diameter) uniformly distributed around the HA particles were fabricated following the above process. The ability of the coating to kill the bacteria *L. plantarum* was determined, which revealed strong antibacterial properties.

KEYWORDS: Antibacterial polymers, Antibacterial surface coating, Block copolymer synthesis, Hydroxyapatite, Ag nanoparticle

INTRODUCTION

The prevention of bacterial adhesion to surfaces is significant to maintain the function and fidelity of many materials and processes; most importantly, it benefits human health.[1] Once adhered onto a solid surface, bacteria form colonies and subsequent biofilms that serve as reservoirs for the development of pathogenic infections such as tooth decay, and biofouling of medical implants and biomedical devices ultimately leading to implant rejection.[2] Implant-associated infections are among the most serious postsurgical complications from medical device implantation, including prosthetic joints (e.g., hip, knee, and shoulder) and fracture fixation hardware.[3] Infection rates related to orthopedic implants have been reduced to less than 5% owing to strict hygienic protocols and intraoperative systemic prophylactic treatment.[4] However, the overall number of such infections has been continuously increasing with the growing demand for surgical implantation as a result of population aging and increasing participation in recreational activities.[5] Prevention of biofilm formation has therefore been of recent interest to biomaterials researchers, whose efforts have focused on the design of coatings tailored for this purpose.[6] Coating strategies can be classified as passive (antifouling) and active (antimicrobial).[7] Passive strategies rely on inhibition of bacterial attachment, typically through physical prevention of nonspecific cell attachment by a grafted polymer coating, whereas active strategies rely on the presence of an antibacterial compound that actively promotes bacteria death by interfering with biochemical pathways.[8] Various surface modifications have been developed to improve the antibacterial properties of implant surfaces, such as applying bactericidal agents, [9] hydrogels, [10] Ag nanoparticles or compounds, [10a, 11] or various polymers.[12]

Ag is an extremely potent antimicrobial agent that exhibits strong cytotoxicity toward a broad range of microorganisms, while exhibiting low known toxicity in humans.[11a] Ag exhibits

an oligodynamic effect, that is, Ag is capable of causing a bacteriostatic (growth inhibition), or even a bactericidal (antibacterial) effect.[11a] Recently, researchers have reported that Ag nanoparticles exhibited more efficient antibacterial performance compared with their bulk counterparts[13]. Although the debate concerning the mechanisms by which Ag nanoparticles exert their antibacterial action is still underway, it is generally accepted that their mechanism of action involves a release of Ag ions, which then interacts with and kills bacteria. Recently, a hypothesis has been formulated, suggesting that the antibacterial properties of AgNPs can be ascribed to a short distance nanomechanical action involving their direct interaction with the bacterial cell membrane.[14] Thus, it is very promising to introduce Ag nanoparticles on a surface for broad antibacterial applications. However, aggregation of Ag nanoparticles and promoted adhesion of bacteria act as barriers to fabricating surface coatings that exhibit strong antibacterial effects as well as biocompatibility using only Ag nanoparticles.[15] Polymeric materials with great structure tailorability and flexibility have the potential to inhibit aggregation of Ag nanoparticles and form uniform surface coatings on various substrates.[16] These materials can also control the release of Ag ions for sustained antibacterial effects and reduce cytotoxicity.

Hydroxyapatite (HA, $[Ca_{10}(PO_4)_6(OH)_2]$) is a bioactive calcium phosphate ceramic that is the main mineral component of natural bone, teeth, and most of implants for bone repair or regeneration.[17] Generation of biofunctional surfaces on hydroxyapatite that inhibit bacterial growth is one of the best methods to prevent colonies and biofilms on these implants. However, compared with polymeric and noble metal surfaces, a hydroxyapatite surface is difficult to modify by graft polymerization or complexation reaction due to lack of functional groups on the surface. It has been reported that bisphosphonates, structural analogues of naturally existing pyrophosphate with increased chemical and enzymatic stability, have strong affinity for

hydroxyapatite.[18] Moreover, it was also reported that bisphosphonates can inhibit enzymes (metalloproteinases), which degrade the collagen network of bone.[19] In the present paper, we report on the synthesis of a block copolymer composed of bisphosphonate (block 1) and pyridine (block 2). Bisphosphonate oligomers are hypothesized to tether the copolymer on the HA surface. Ag can then be incorporated into this system due to strong coordination capability of pyridine oligomers. We describe as being scorpion-like -- the bisphosphonate-containing block acts like the scorpion's legs, securing the polymer to the surface; while the pyridine/Ag block acts like the scorpion's tail, which can kill bacteria. After careful structural analysis and polymer characterization, the antibacterial properties of the polymer-Ag and the HA surface modified by the polymer-Ag were studied. Lactobacillus plantarum (*L. plantarum*) was selected as model bacteria, which are prominent in decaying plant material and teeth. [20]

EXPERIMENTAL SECTION

Materials. 2,2'-Azobis(2-methylpropionitrile) (AIBN) was purified by recrystallization in methanol. *L. plantarum* was purchased from Custom Probiotics Inc. (Glendale, California). All other chemicals were purchased from Sigma-Aldrich and used as received.

Synthesis of 2-(dodecylthiocarbonothioylthio)-2-methylpropanoic acid (RAFT-COOH)

1-Dodecanethiol (8.076 g, 0.040 mol), acetone (19.2 g, 0.331 mol), and Aliquot 336 (tricaprylylmethylammonium chloride, 0.649 g, 0.0016 mol) were mixed in a 250 mL flask cooled to 10 °C under N_2. Sodium hydroxide solution (50%) (3.354 g, 0.042 mol) was added over 20 min. The reaction was stirred for an additional 15 min before carbon disulfide (3.042 g, 0.040 mol) in acetone (4.036 g, 0.069 mol) was added over 20 min, during which time the color turned red. Ten minutes later, chloroform (7.125 g, 0.060 mol) was added in one portion,

followed by drop wise addition of 50% sodium hydroxide solution (16 g, 0.2 mol) over 30 min. The reaction was stirred overnight. 60 mL of water was added, followed by 10 mL of concentrated HCl to acidify the aqueous solution. N_2 was purged through the reactor with vigorous stirring to help evaporate off acetone. The solid was collected with a Buchner funnel and then stirred in 100 mL of 2-propanol. The undissolved solid was filtered off. The 2-propanol solution was concentrated to dryness, and the resulting solid was recrystallized from hexanes to afford 9.25 g of yellow crystalline solid. Yield: 63.5%. ^{1}H NMR: 0.99 (t, 3 H), 1.35-1.46 (m, 20 H), 1.76 (s, 6 H), 3.42 (t, 2H), 13.12 (s, 1H). MS (M + Na^+, chem): calcd: 387.2. Found: 387.2.

Synthesis of Tetraethyl (*N*,*N*-Dibenzyl)aminomethyl-bis(phosphonate) (TEBAP)

Diethyl phosphite (12.8 g, 93 mmol), triethyl orthoformate (5.3 g, 35.5 mmol), and dibenzylamine (5.9 g, 30 mmol) were mixed in a 100 mL three-necked round-bottom flask. The solution was heated at 150 ^{o}C under N_2 atmosphere for 5 h. After cooling to RT, the mixture was dissolved in $CHCl_3$ (250 mL) and the solution was washed with 3 × 60 mL of 5% aqueous NaOH and 2 × 75 mL of brine. The organic fraction was dried with anhydrous Na_2SO_4, and then the solvents were removed by rotary evaporation. The resulting oil was purified by column chromatography. Yield: 52%. ^{1}H NMR ($CDCl_3$, ppm): δ 1.36 (t, 12H, -CH_3), 3.58 (t, 1H, P-CH-P), 4.07 (m, 4H, N-CH_2-Ph), 4.21 (m, 8H, O-CH_2-), 7.20-7.45 (m, 10H, Ar-H). ^{31}P NMR ($CDCl_3$, 300 MHz): δ 20.7 (s). MS: calcd 506.5, obsd 506.5 (M + Na^+).

Synthesis of Tetraethyl Aminomethyl-bis(phosphonate)

A 250 mL three necked round-bottom flask was flushed with N_2 and charged with 10% Pd/C (0.5 g), and a solution of TEBAP (5.0 g, 10.4 mmol) in EtOH (150 mL) was added. The mixture was refluxed with vigorous stirring under H_2 atmosphere for 24 h. After filtration and evaporation of volatiles, the product was obtained as colorless liquid. Yield: 93%. ^{1}H NMR

($CDCl_3$, ppm): δ 1.36 (t, 12H, -CH_3), 3.43 (t, 1H), 4.23 (m, 8H, O-CH_2-). ^{31}P NMR ($CDCl_3$, ppm): δ 20.8 (s). MS: calcd 326.2, obsd 326.2 (M + Na^+).

Synthesis of Monomer (AABP)

To a solution of tetraethyl aminomethyl-bis(phosphonate) (0.606 g, 2.00 mmol) and triethylamine (0.42 mL, 3.00 mmol) in anhydrous dichloromethane (5.60 mL) was added acryloyl chloride (0.32 mL, 3.30 mmol) in anhydrous dichloromethane (3.26 mL) at 0 ^oC, under N_2 and the resulting mixture was stirred at room temperature for 2 h. The reaction was stopped by addition of distilled water (3.26 mL). The organic layer was washed with distilled H_2O (25 mL), 2M HCl (25 mL), saturated $NaHCO_3$ (25 mL), and distilled H_2O (25 mL) and dried over anhydrous Na_2SO_4 and filtered. After removal of the solvent, the crude product was purified by reversed-phase flash chromatography on Silica, eluting with H_2O:MeOH (50:50) to give monomer as a white solid. Yield: 48%.

^{1}H NMR ($CDCl_3$, ppm): δ 1.30-1.36 (m, 12 H, -CH_3), 4.2 (m, 8 H, P-O-CH_2-), 5.10-5.15 (d, 1H, CH-P), 5.15-5.19 (q, 1H, =CH), 5.71-5.74, 5.30 (q, 2H, =CH_2). ^{31}P NMR ($CDCl_3$, ppm): 16.11 (s). MS calcd 348.1, obsd 348.1 (M + Na^+)

Synthesis of Bisphosphonate Oligomers (p(BP))

The polymer was denoted as p(BP). To a 10-mL round-bottom flask, 0.97 g AABP (2.73 mmol), 0.0030 g AIBN (1:5 molar ratio to RAFT-COOH), 0.0328 g RAFT-COOH (0.091mmol) and 2 mL DMF were added and stirred at room temperature until they were completely dissolved. The solution was sparged with nitrogen gas for 20 min and then heated to 65 ^oC for 4 h. The reaction was terminated by quenching in an ice-water bath to reduce the temperature. The reaction solution was dialyzed against DI water for 3 days to remove solvent and the unreacted monomer. The yellow solid was dried in vacuo for 12 h. ^{1}H NMR ($DCCl_3$, ppm): 2.98 (4H, m, N-CH_2 and

S-CH_2), 2.83 (6 H, N-CH_3), 2.60 (2 H, S-CH_2), 2.12 (2H, m, CH_2), 1.76 (2 H, m, CH_2), 1.24 (34 H, m, CH_2), 0.85 (3H, t, CH_3).

Synthesis of p(BP-b-VP) Block Copolymer

p(BP) (5 kDa target molecular weight) was used as macro RAFT agent to synthesize p(BP-b-VP) diblock copolymers. p(BP), 2-vinylpyridine, AIBN, chlorobenzene and stir-bar were added to a round-bottom flask and sealed with a rubber septum. The contents were degassed by sparging with dry nitrogen for 20 min. The polymerization was initiated by placing the flask in an oil bath at 70 ^{o}C. After 6 h reaction, the polymerization was terminated by quenching the flask in ice water and precipitating the polymer in methanol. The polymer was dried under vacuum.

Surface Modification of HA with p(BP-b-VP) Block Polymer (HA-p(BP-b-VP))

A 5 mg/mL of p(BP-b-VP) solution was prepared by dissolving 50 mg p(BP-b-VP) in a 10 mL H_2CCl_2. Dried HA was immersed in the polymer solution with shaking for 24 h. The modified HA was then added to centrifuge tubes and purified via centrifugation at ~8300 rcf to form a pellet, followed by removal of the supernatant and resuspension with H_2CCl_2. This process was repeated 4x. The pure sample was stored in a dust free environment at room temperature until use.

Preparation of p(BP-b-VP) Membrane on Glass Slide (p(BP-b-VP-G))

The p(BP-b-VP) solution (1 mg/mL) was prepared by dissolution of p(BP-b-VP) in $HCCl_3$. The solution was then filtered through a 0.45-μm Teflon syringe filter and cast onto a clean glass substrate by simply adding drops of the solution to the glass. The membranes were slowly dried at RT for 12 h and then *in vacuo* for 12 h. These were indicated as p(BP-b-VP-G).

Preparation of p(BP-b-VP) containing Ag nanoparticles (p(BP-b-VP-Ag^0))

The p(BP-b-VP) block copolymer, HA-p(BP-b-VP), and p(BP-b-VP)-G were added to aqueous $AgNO_3$ (20 mL, 5.0 mmol L^{-1}) solutions for 24 h to allow the pyridine groups to complex the Ag^+. The samples were subsequently washed thoroughly with water (200 mL) and stored in DI water for 12 h to remove any excess $AgNO_3$. An excess of aqueous $NaBH_4$ was then added with vigorous stirring, then the mixture was kept at RT for 12 h. The resultant Ag nanoparticles containing materials were washed copiously with DI water and stored in 500 mL DI water, and dried under vacuum at 80 °C for 12 h. These samples were stored in a dust free environment at room temperature until use. They abbreviations used to indicate Ag nanoparticles were present are: p(BP-b-VP)-Ag^0 for p(BP-b-VP) block copolymer with Ag nanoparticles, HA-p(BP-b-VP)-Ag^0 for HA-p(BP-b-VP) with Ag nanoparticles, and p(BP-b-VP)-G-Ag^0 for p(BP-b-VP)-G with Ag nanoparticles.

Control Experiment

HA was soaked in aqueous $AgNO_3$ (20 mL, 5.0 mmol L^{-1}) solutions for 24 h. The sample was subsequently washed thoroughly with water (200 mL) 6 times and stored in DI water for 12 h to remove any excess $AgNO_3$. An excess of aqueous $NaBH_4$ was then added with vigorous stirring, then the mixture was kept at RT for 12 h. The resultant material was washed copiously with DI water and stored in 500 mL DI water, and dried under vacuum at 80 °C for 12 h. The sample was named as HA-C.

Ag leaching experiment

0.1 g p(BP-b-VP)-Ag^0 was soaked in DI for 2 weeks at room temperature. After filtration, the concentration of Ag in the filtrate was tested by inductively coupled plasma mass spectrometer (ICP-MS).

Antimicrobial Activity Assay

Antimicrobial activity of the generated materials was evaluated using *L. plantarum*. A colony of *L. plantarum* bacteria was cultivated in Luria−Bertani broth (containing 10 g/L peptone, 10 g/L sodium chloride, and 5 g/L yeast extract) at 37 °C, shaking at 160 rpm for 24 h. The bacteria were diluted with 0.1 mol/L phosphate buffer solution (PBS, pH = 7) to the desired concentration. A certain amount of HA and HA-p(BP-b-VP)-Ag^0 were immersed in the bacterial suspension, then shaken at 37 °C for 20 h. After an overnight culture at 37 °C, colony forming units (CFU) of *L. plantarum* was determined (using BioMate 3S Spectrophotometer) from the measured absorbance at 600 nm wavelength using previously established standard calibration curves. A certain amount of suspension was taken, diluted appropriately, and plated on L-agar plates for 20 h incubation. Theoretically, each surviving bacterium develops into a distinct colony after incubation, and the number of viable bacteria referred to as colony forming units (CFU), thus providing a direct measure of bacterial viability. A bacterial suspension then was sprayed onto a p(BP-b-VP)-Ag film on glass slide or a blank glass slide (no modification) in a fume hood by using a commercial chromatography sprayer (VWR Scientific) (spray rate of 10 mL/min). After drying for 10 min under air, the slide was placed in a Petri dish, and then growth agar (0.7% agar in a yeast dextrose broth, autoclaved, and cooled to 37°C) was added. The Petri dish was closed, sealed, and incubated at 37°C overnight. The surface of samples was washed using DI water to remove the dead and unattached bacteria. Bacteria remaining on the sample surfaces were stained with fluorescein (Na salt) according to standard protocol. The bacteria cells on the surface were imaged using a Nikon Eclipse 80i microscope with 100x lens through a FITC filter. Photographs were taken with a CCD-Cool SNAP camera (Roper scientific, Inc., USA).

Characterization

^{1}H NMR was collected on a Varian Unity spectrometer at 400 MHz at 30°C with

tetramethylsilane (TMS) as the internal standard. Thermogravimetric analyses (TGA) was done with a Perkin Elmer TGA-2 thermogravimetric analyzer (Inspiratech 2000 Ltd., UK) at a heating rate of 10 °C/min. All the samples were first vacuum-dried and kept in the TGA furnace at 150°C in a nitrogen atmosphere for 30 min to remove water before TGA characterization. Transmission electron microscopy (TEM) was carried out on a Jeol JEM 2000EXII operating at 200 kV. Differential scanning calorimetric (DSC) experiments were carried out under a nitrogen atmosphere using a Perkin Elmer DSC-7 system at a heating rate of 10 ^{o}C/min. Wide-angle X-ray diffraction (XRD) measurements were obtained on a Rigaku Max 2500 V PC X-ray diffract meter (Japan) with Cu-K_{α} radiation (40 kV, 200 mA) with a scanning rate of 8 ^{o}C/min. X-ray photoelectron spectroscopy (XPS) analysis of the samples was performed using a Thermo Scientific K-Alpha ESCA instrument equipped with aluminum $K_{\alpha 1,2}$ monochromatized radiation at 1486.6 eV X-ray source. For Ag determination, ICP-MS (Elan DRC II (Perkin–Elmer SCIEX, Norwalk, CT, USA)) was used.

RESULTS AND DISCUSSION

Synthesis

The monomer AABP was synthesized from the reaction of acryloyl chloride and tetraethyl aminomethyl-bis(phosphonate) (Scheme 1). The latter was prepared by reaction of dibenzylamine, triethylorthoformate, and diethyl phosphite to give the intermediate TEBAP, followed by debenzylation with H_2 and Pd/C as the catalyst. The deprotected tetraethyl aminomethyl-bis(phosphonate) was converted quantitatively into monomer AABP by means of a substitution reaction with an excess of chloroacetyl chloride. The AABP structure was confirmed by ^{1}H and ^{31}P NMR, and mass spectrometry (MS) (in experimental).

Bisphosphonate oligomers were synthesized by RAFT polymerization in DMF at 70 ^{o}C using AABP as the monomer, RAFT-COOH as the chain transfer agent and AIBN as the initiator as shown in Scheme 1. Figure 1 shows ^{1}H NMR spectra of AABP and p(BP). Three peaks of AABP at 5.15, 5.71 and 5.30 ppm were assigned to the vinyl group protons. After polymerization, these three peaks disappeared and a new peak in 0.92 ppm appeared which was attributed to the proton in the end methyl group of the RAFT-COOH reagent. The number of repeat units of bisphosphonate can be calculated by the integration ratio of the peak at 4.22 ppm (O-CH_2-) and 0.92 ppm (CH_3-in RAFT-COOH). The calculated repeated units of p(BP) by ^{1}H NMR was 28, which is close to the repeat unit target (30). As shown in Figure 2, ^{31}P NMR spectra of AABP and p(BP) exhibit similar chemical shifts around 16.1 ppm for AABP and 17.0 for p(BP) which were attributed to P of phosphonate. The small difference comes from the different P chemical environment in monomer and polymer.

Subsequently, the p(BP) oligomer was used as a macro-chain transfer agent, and 2-vinylpyridine was selected as monomer, for the synthesis of p(BP-b-VP) block copolymers. After the polymerization, the polymer was precipitated into water to remove solvent, unreacted p(BP), and 2-vinylpyridine. As shown in Figure 1, compared with ^{1}H NMR of p(BP), four new peaks in ^{1}H NMR of p(BP-b-VP) appear between 6.31ppm and 8.30 ppm that were attributed to the pyridine protons. 100 pyridine repeated units were added, as determined by ^{1}H NMR integration ratio calculation of the peak at 6.31ppm to that at 4.22 ppm. These two polymers exhibited similar chemical shifts of ^{31}P NMR at 17.0 ppm, which also approve successful synthesis of p(BP-b-VP), as shown in Figure 2.

Thermal properties

The thermal stabilities of the p(BP) and p(BP-b-VP) were analyzed by TGA under flowing nitrogen (Figure 3). These samples were preheated to 150 °C and held isothermally for 30 min for moisture removal. The initial weight loss of p(BP) and p(BP-b-VP) was observed at 250 ^{o}C and was assigned to the decomposition of the phosphonate group.[21] The initial 5% weight loss temperature of p(BP) ranged from 250 ^{o}C to 264 ^{o}C, which is lower than that of p(BP-b-VP) (from 250 ^{o}C to 285 ^{o}C). The residue of p(BP-b-VP) at 600 ^{o}C remained 17% which was attributed to the carbonization of pyridine groups. Pyridine oligomer increased thermal stability of polymer. From the thermal testing, it can be concluded that the p(BP-b-VP) would meet the thermal stability requirements for antibacterial surface coating applications.

In order to further investigate the basic properties of p(BP-b-VP), the glass transition temperature was characterized by DSC. For comparison, the thermal property of p(BP) was also tested and shown in Figure 4. In order to eliminate the thermal history, the DSC curves of the second scan were recorded. No melting point was observed for the two polymers, which means they are amorphous. The glass transition temperatures (T_g) of p(BP-b-VP) is at 92 ^{o}C, which can be assigned to the presence of strong polar pyridine oligomer.

p(BP-b-VP)-Ag^{0}

Since we showed that p(BP-b-VP) could be synthesized, we went on to develop it as an antibacterial polymer and ultimately a coating. To accomplish this, the polymer was exposed to Ag^{+}, which was complexed by the pyridine groups. The Ag^{+} is subsequently reduced by exposure to $NaBH_4$ to obtain Ag nanoparticles. This is shown in Scheme 1. ICP-MS analysis confirmed that the amount of Ag^{+} that was loaded into p(BP-b-VP) is 29.8% (weight percent). The Ag^{+} containing polymer was named as p(BP-b-VP)-Ag^{+}. ICP-MS analysis also revealed that the Ag content was ~25.7% after the $NaBH_4$ reduction process. XPS was also used to confirm

the presence of Ag in the polymer after reduction by analyzing the Ag $3d_{3/2}$ and Ag $3d_{5/2}$ regions, as these regions are very sensitive to the chemical environment surrounding the Ag and can provide important information to distinguish between Ag ions and metallic Ag.[11a] This data is shown in Figure 5, which reveals the Ag $3d_{3/2}$ at 373.9 eV and Ag $3d_{5/2}$ 367.9 eV for Ag^+. These peaks shift to 373.6 and 367.6 eV through the reduction process, which is characteristic of Ag $3d_{3/2}$ and $3d_{5/2}$ Ag nanoparticle respectively.[22]

XRD was also conducted on p(BP-b-VP), p(BP-b-VP)-Ag^+ and p(BP-b-VP)-Ag^0, and the data is shown in Figure 6. The curves of p(BP-b-VP) and p(BP-b-VP)-Ag^+ were broad and without obvious peak features, which also indicated that they were all amorphous. The p(BP-b-VP)-Ag^0 displayed a new peak at $2\theta = 38.4°$ which is the characteristic (1, 1, 1) plane of face-centered cubic crystalline Ag.[23] This confirms the formation of crystalline Ag in p(BP-b-VP) matrix by the reduction of Ag^+. Figure 7 shows TEM micrographs of p(BP-b-VP)-Ag^+ and p(BP-b-VP)-Ag^0. The TEM image of p(BP-b-VP)-Ag^0 revealed that this sample is constituted by well-dispersed Ag nanoparticles with diameters of 5-15 nm. In order to investigate leaching of Ag from p(BP-b-VP)-Ag^0, the polymer was stored in DI water for 2 weeks and the solution was analysized by ICP-MS. Very low Ag leaching was detected (0.3 ppm), indicating that the Ag nanoparticles were stable in p(BP-b-VP)-Ag^0.

The antibacterial properties of p(BP-b-VP)-Ag^0 were determined by the standard disk diffusion assay according to the procedure on Luria Bertani agar medium reported by Elgayyar et al.[24] In these tests *L. plantarum* was used as model bacteria. *L. plantarum* is a gram positive bacterium that is found in dairy, meat, many vegetable fermentations, and the mouth, which can break down sugars as part of their metabolism, forming lactic acid and promoting tooth (main mineral component: HA) decay.[25] All bactericidal activity tests were performed on tests discs of

11 mm diameter and 0.3 mm thickness. The disc of p(BP-b-VP)-Ag^0 was very efficient as an antibacterial agent, which can create a large zone of inhibition in the bacterial growth lawn, as shown in Figure 8. The disc of p(BP-b-VP) and blank (just *L. plantarum* was added in the dish) were also tested as controls. The growth bacteria filled all of these disc areas and covered the p(BP-b-VP) surface, with no inhibition zone forming, which implies that these discs have no antibacterial activity.

p(BP-b-VP)-Ag^0 on glass slide and antibacterial properties

In order to investigate this system's practical application as an antibacterial coating, a compact and smooth p(BP-b-VP) film with thickness of 2.5 μm was prepared on a glass slide using a solution casting method,[26] as shown in Figure 9. Then, Ag nanoparticles were incorporated into film. The p(BP-b-VP)-Ag^0 film was used for antibacterial test with a blank slide used as control. A suspension of *L. plantarum* (1×10^6 CFU mL^{-1}) was sprayed onto the respective modified and unmodified glass slides using a commercial chromatography sprayer (VWR Scientific) (spray rate of 5 mL/min). After being air dried, the slides were placed in Petri dishes, and then growth agar (0.7% agar in a yeast/dextrose broth) was added. The Petri dishes were sealed, and incubated for 20 h at 37°C. Then, the slides were taken out, washed with H_2O to remove agar and unattached *L. plantarum*, and exposed to fluorescein sodium salt (according to standard protocol). Figure 10 shows representative microscope images of the fluorescently stained *L. plantarum* attached to the surfaces of the p(BP-b-VP)-Ag^0 modified glass slide, and the control. A high bacteria density at the glass slide surface was observed, while no bacteria was observed on the surface of p(BP-b-VP)-Ag^0 film, this clearly shows the antibacterial properties of the p(BP-b-VP)-Ag^0 film. After being incubated for 3 days, several visible bacterial colonies

appeared on glass slide surface, as shown in Figure 11. While, no bacterial colonies were observed on the p(BP-b-VP)-Ag^0 film.

HA containing p(BP-b-VP)-Ag^0 and antibacterial properties

Next, we wanted to prove that the p(BP-b-VP)-Ag^0 could be deposited on HA surfaces. To accomplish this HA particles were immersed into p(BP-b-VP) solution at room temperature, then washed three times by fresh H_2CCl_2 to remove unattached polymer. TEM analysis revealed that a thin and uniform polymer layer (～4 nm) was formed around the HA due to strong interaction of p(BP-b-VP) and HA, as shown in Figure 12. Then, the substrate (HA- p(BP-b-VP)) was immersed into dilute $AgNO_3$ solution, whereupon Ag ions were bound to the polymer coating on HA. Finally, Ag ions were reduced into Ag nanoparticles by exposure to $NaBH_4$. Figure 12(c) illustrates the TEM image of HA-p(BP-b-VP)-Ag nanoparticles. Ag nanoparticles with the diameters of 5-15 nm deposited on the surfaces of HA particles. The well-dispersed distribution of Ag nanoparticles indicates that the aggregation problem of Ag nanoparticles has been avoided, which can result in large surface area and great antibacterial property. In order to evaluate the function of polymer in the process, sample HA-C was prepared by exposing HA to Ag^+ without previous p(BP-b-VP) exposure. The TEM image of HA-C is shown in Fig. 12(d). As can be seen, no Ag nanoparticles were observed on the HA, indicating that p(BP-b-VP) played a key role in generating Ag nanoparticles on the HA to render them antibacterial.

A certain amount of HA-p(BP-b-VP)-Ag^0 was added to *L. plantarum* solution in yeast/dextrose broth. The suspension was shaken for 10 min, and then incubated at 37°C for 20 h. For comparison purposes, the unmodified HA, HA-C and blank experiment (nothing added to bacteria solution) were also conducted in the same conditions. Figure 13 displayed the optical

images of these samples after 20 h culture at 37 ^{o}C. The solution of HA, HA-C and blank become cloudy resulting from *L. plantarum* growth. All of HA- p(BP-b-VP)-Ag nanoparticles treated solution remained clear and transparent, which indicated the growth of *L. plantarum* was inhibited. The concentration of *L. plantarum* was tested by absorbance measurement at 600 nm wavelength, and the results were showed in Figure 14. The concentration of *L. plantarum* solution treated by HA- p(BP-b-VP)-Ag nanoparticles ranged from 1.99×10^8 CFU mL^{-1} to 2.36×10^8 CFU mL^{-1} with the HA- p(BP-b-VP)-Ag content increasing from 0.5% to 1.0%. These values are close to the original *L. plantarum* concentration (1.71×10^8 CFU mL^{-1}). The concentration of *L. plantarum* solution treated by HA, HA-C and blank increased from 1.71×10^8 CFU mL^{-1} to 1.85×10^9 CFU mL^{-1}, 1.74×10^9 CFU mL^{-1} and 1.86×10^9 CFU mL^{-1}, respectively, which are almost 10 times larger than these of HA- p(BP-b-VP)-Ag nanoparticles treated solution (Figure 14). These indicated that the HA- p(BP-b-VP)-Ag nanoparticles exhibited excellent antibacterial property. In order to investigate the *L. plantarum* activity after treated by HA and HA- p(BP-b-VP)-Ag nanoparticles, the *L. plantarum* solutions with same concentration (2×10^6 CFU mL^{-1}) were prepared from above samples. 0.1 mL *L. plantarum* solution was painted on the surface of nutrient agar media, and then samples were incubated for 20 h at 37 ^{o}C. The result was showed in Figure 15. In this manner, clear non-growth *L. plantarum* was observed in the agar experiments from the solution treated by HA-p(BP-b-VP)-Ag nanoparticles, which indicated that the *L. plantarum* was inactivated. On the other hand, *L. plantarum* colonies covered all of agar surface when HA and HA-C treated, and blank *L. plantarum* was used.

CONCLUSION

In this submission we synthesized a novel block copolymer that was capable of adhering to HA surfaces, as well as complexing Ag^+. The polymer was characterized by NMR, TGA, XRD, XPS, TEM, and microscopy. The purpose of synthesizing such a polymer was to allow HA-containing medical devices, implants, and teeth to be coated with the polymer, while the Ag^+ could be reduced to Ag^0, allowing the surfaces to be rendered antibacterial. Through our processing, we were able to modify HA surfaces with polymer layers of ~ 4 nm, and Ag nanoparticles of 5-15 nm in diameter. We showed that the polymer, and the polymer-coated surfaces (with Ag nanoparticles) were able to kill the bacteria *L. plantarum* very effectively. We feel that these polymers have promise for future use as antibacterial coatings for a wide variety of HA surfaces, while the concept can be adapted for a variety of other materials.

Acknowledgements

MJS acknowledges funding from the University of Alberta (the Department of Chemistry and the Faculty of Science), the Natural Sciences and Engineering Research Council of Canada (NSERC), the Canada Foundation for Innovation (CFI), and the Alberta Advanced Education & Technology Small Equipment Grants Program (AET/SEGP).

References

1. (a) Neoh, K. G.; Hu, X.; Zheng, D.; Kang, E. T., *Biomaterials* **2012,** *33*, 2813-2822; (b) Wang, B.; REN, K.; Chang, H.; Wang, J.; Ji, J., *ACS Appl. Mater. Interfaces* **2013,** *34*, 4136-4143.
2. (a) Donlan, R. M.; Costerton, J. W., *Clin. Microbiol. Rev.* **2002,** *15*, 167-193; (b) Costerton, J.; Stewart, P. S.; Greenberg, E., *Science* **1999,** *284*, 1318-1322; (c) McLean, R. J.; Nickel, J. C.; Cheng, K.-J.; Costerton, J. W.; Banwell, J. G., *Crit. Rev. Microbiol.* **1988,** *16*, 37-79.
3. (a) Engemann, J. J.; Carmeli, Y.; Cosgrove, S. E.; Fowler, V. G.; Bronstein, M. Z.; Trivette, S. L.; Briggs, J. P.; Sexton, D. J.; Kaye, K. S., *Clin. Infect. Dis.* **2003,** *36*, 592-598; (b) Zimmerli, W.; Ochsner, P., *Infection* **2003,** *31*, 99-108.
4. O'Driscoll, S. W.; Fitzsimmons, J. S., The role of periosteum in cartilage repair. *Clin. Orthop. Related Res.* **2001,** *391*, S190-S207.
5. Smeeth, L.; Thomas, S. L.; Hall, A. J.; Hubbard, R.; Farrington, P.; Vallance, P., Risk of myocardial infarction and stroke after acute infection or vaccination. *N. Engl. J. Med.* **2004,** *351*, 2611-2618.
6. (a) Banerjee, I.; Pangule, R. C.; Kane, R. S., *Adv. Mater.* **2011,** *23*, 690-718; (b) Li, M.; Neoh, K. G.; Kang, E. T.; Lau, T.; Chiong, E., *Adv. Funct. Mater.* **2014,** *24*, 1631-1643; (c) Yang, W. J.; Cai, T.; Neoh, K.-G.; Kang, E.-T.; Teo, S. L.-M.; Rittschof, D., *Biomacromolecules* **2013,** *14*, 2041-2051; (d) Venault, A.; Yang, H.-S.; Chiang, Y.-C.; Lee, B.-S.; Ruaan, R.-C.; Chang, Y., *ACS Appl. Mater. Interfaces* **2014,** *6*, 3201-3210; (e) Ng, V. W. L.; Tan, J. P. K.; Leong, J.; Voo, Z. X.; Hedrick, J. L.; Yang, Y. Y., *Macromolecules* **2014,** *47*, 1285-1291; (f) García‐Fernández, L.; Cui, J.; Serrano, C.; Shafiq, Z.; Gropeanu, R. A.; Miguel, V. S.; Ramos, J. I.; Wang, M.; Auernhammer, G. K.; Ritz, S., *Adv. Mater.* **2013,** *25*, 529-533.
7. Sileika, T. S.; Kim, H.-D.; Maniak, P.; Messersmith, P. B., Antibacterial performance of polydopamine-modified polymer surfaces containing passive and active components. *ACS Appl. Mater. Interfaces* **2011,** *3*, 4602-4610.
8. Lienkamp, K.; Tew, G. N., *Chem-Eur J* **2009,** *15*, 11784-11800.
9. Gurumurthy, M.; Rao, M.; Mukherjee, T.; Rao, S. P. S.; Boshoff, H. I.; Dick, T.; Barry, C. E.; Manjunatha, U. H., *Mol. Microbiol.* **2013,** *87*, 744-755.
10. (a) Liu, Y.; Ma, W.; Liu, W.; Li, C.; Liu, Y.; Jiang, X.; Tang, Z., *J. Mater. Chem.* **2011,** *21*, 19214-19218; (b) Hu, R.; Li, G.; Jiang, Y.; Zhang, Y.; Zou, J.-J.; Wang, L.; Zhang, X., *Langmuir* **2013,** *29*, 3773-3779.
11. (a) Shah, M. S. A. S.; Nag, M.; Kalagara, T.; Singh, S.; Manorama, S. V., *Chem. Mater.* **2008,** *20*, 2455-2460; (b) Gutman, O.; Natan, M.; Banin, E.; Margel, S., *Biomaterials* **2014,** *35*, 5079-5087; (c) Park, J.; Kim, J.; Singha, K.; Han, D.-K.; Park, H.; Kim, W. J., *Biomaterials* **2013,** *34*, 8766-8775; (d) Jin, G.; Qin, H.; Cao, H.; Qian, S.; Zhao, Y.; Peng, X.; Zhang, X.; Liu, X.; Chu, P. K., *Biomaterials* **2014,** *35*, 7699-7713.
12. (a) Yuan, W.; Wei, J.; Lu, H.; Fan, L.; Du, J., *Chem. Commun.* **2012,** *48*, 6857-6859; (b) Sun, T.; Wang, G.; Feng, L.; Liu, B.; Ma, Y.; Jiang, L.; Zhu, D., *Angew. Chem. Int. Ed.* **2004,** *43*, 357-360; (c) Sileika, T. S.; Barrett, D. G.; Zhang, R.; Lau, K. H. A.; Messersmith, P. B., *Angew. Chem. Int. Ed.* **2013,** *52*, 10766-10770.
13. Fan, Z.; Liu, B.; Wang, J.; Zhang, S.; Lin, Q.; Gong, P.; Ma, L.; Yang, S., *Adv. Funct. Mater.* **2014**, *24*, 3933-3943.
14. Taglietti, A.; Arciola, C. R.; D'Agostino, A.; Dacarro, G.; Montanaro, L.; Campoccia, D.; Cucca, L.; Vercellino, M.; Poggi, A.; Pallavicini, P.; Visai, L., *Biomaterials* **2014,** *35*, 1779-1788.
15. (a) Agarwal, A.; Weis, T. L.; Schurr, M. J.; Faith, N. G.; Czuprynski, C. J.; McAnulty, J. F.; Murphy, C. J.; Abbott, N. L., *Biomaterials* **2010,** *31*, 680-690; (b) Guo, L.; Yuan, W.; Lu, Z.; Li, C. M., *Colloids and Surfaces A: Physicochem. Eng. Aspects* **2013,** *439*, 69-83.
16. (a) Fei, X.; Jia, M.; Du, X.; Yang, Y.; Zhang, R.; Shao, Z.; Zhao, X.; Chen, X., *Biomacromolecules* **2013,** *14*, 4483-4488; (b) Chen, M.; Zhao, Y.; Yang, W.; Yin, M., *Langmuir* **2013,** *29*, 16018-16024; (c) Reithofer, M. R.; Lakshmanan, A.; Ping, A. T.; Chin, J. M.; Hauser, C. A., *Biomaterials* **2014,** *35*, 7535-

7542; (d) Epa, V.; Hook, A.; Chang, C.; Yang, J.; Langer, R.; Anderson, D.; Williams, P.; Davies, M.; Alexander, M.; Winkler, D., *Adv. Funct. Mater.* **2014,** *24*, 2085-2093.
17. (a) Hoang, Q. Q.; Sicheri, F.; Howard, A. J.; Yang, D. S., *Nature* **2003,** *425*, 977-980; (b) Yamagishi, K.; Onuma, K.; Suzuki, T.; Okada, F.; Tagami, J.; Otsuki, M.; Senawangse, P., *Nature* **2005,** *433*, 819-819.
18. Zhang, S.; Gangal, G.; Uludağ, H., *Chem. Soc. Rev.* **2007,** *36*, 507-531.
19. (a) Senaratne, S. G.; Colston, K. W., *Breast Cancer Res.* **2001,** *4*, 18; (b) Fournier, P.; Boissier, S.; Filleur, S.; Guglielmi, J.; Cabon, F.; Colombel, M.; Clézardin, P., *Cancer Res.* **2002,** *62*, 6538-6544.
20. Schultz, M.; Veltkamp, C.; Dieleman, L. A.; Grenther, W. B.; Wyrick, P. B.; Tonkonogy, S. L.; Sartor, R. B., *Inflamm. Bowel Dis.* **2002,** *8*, 71-80.
21. Price, D.; Cunliffe, L. K.; Bullett, K. J.; Hull, T. R.; Milnes, G. J.; Ebdon, J. R.; Hunt, B. J.; Joseph, P., *Polym. Degrad. Stab.* **2007,** *92*, 1101-1114.
22. Thiel, J.; Pakstis, L.; Buzby, S.; Raffi, M.; Ni, C.; Pochan, D. e. J.; Shah, S. I., *Small* **2007,** *3*, 799-803.
23. Southward, R. E.; Thompson, D. W.; St. Clair, A. K., *Chem. Mater.* **1997,** *9*, 501-510.
24. Elgayyar, M.; Draughon, F.; Golden, D.; Mount, J., *J. Food Prot.* **2001,** *64*, 1019-1024.
25. Huang, J.; Wong, H.-L.; Zhou, Y.; Wu, X.; Grad, H.; Komorowski, R.; Friedman, S., *J. Control. Release* **2000,** *67*, 293-307.
26. Zhang, Q.; Zhang, Q.; Wang, J.; Zhang, S.; Li, S., Synthesis and alkaline stability of novel cardo poly (aryl ether sulfone) s with pendent quaternary ammonium aliphatic side chains for anion exchange membranes. *Polymer* **2010,** *51* (23), 5407-5416.

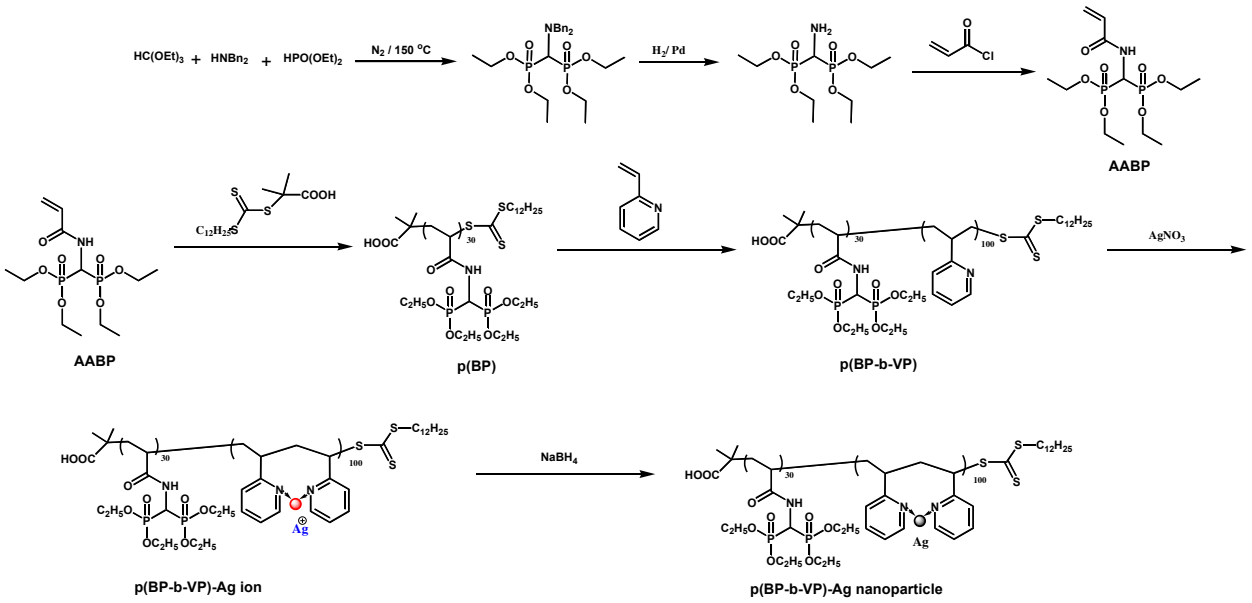

Scheme 1. The synthetic scheme for the monomer and block copolymer.

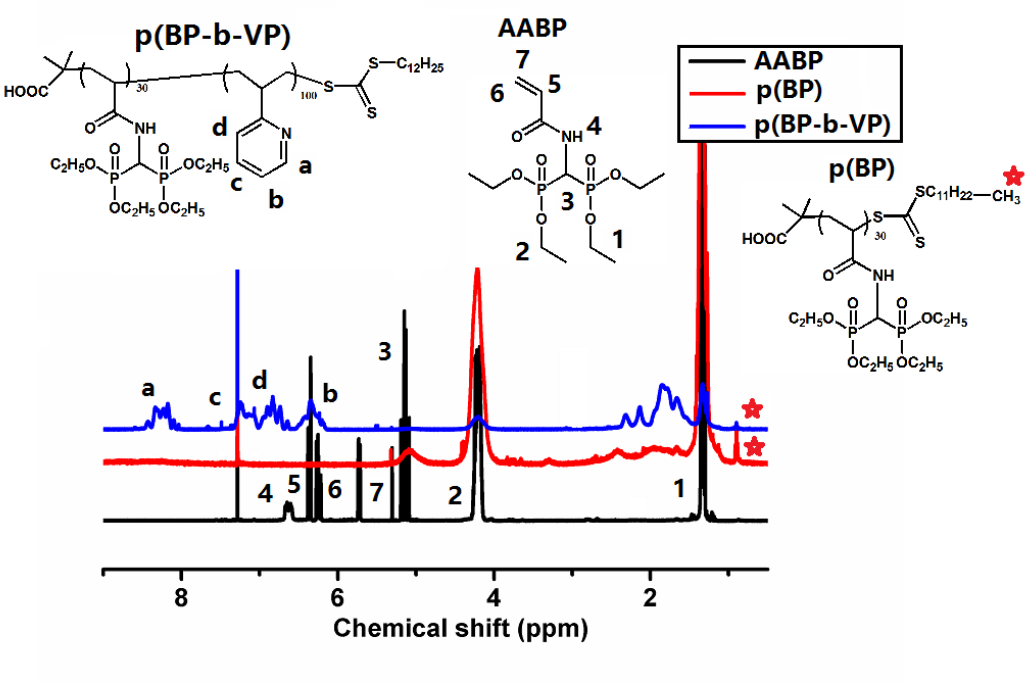

Figure 1. ^{1}H NMR of (black) AABP, (red) p(BP), and (blue) p(BP-b-VP).

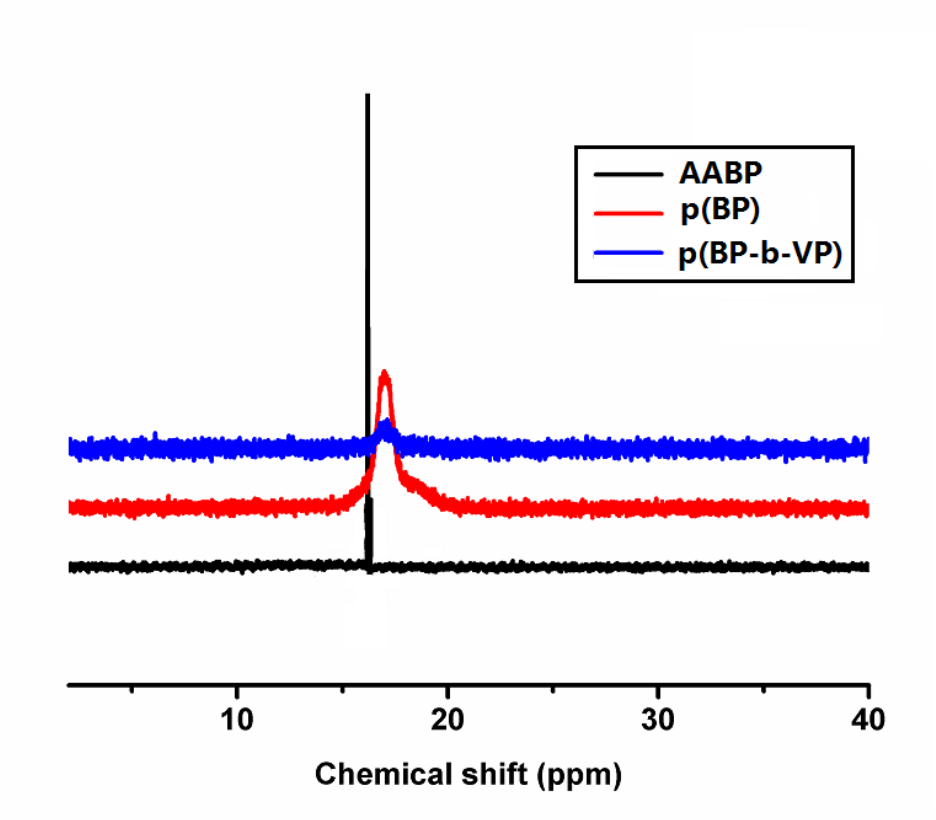

Figure 2. ^{31}P NMR of (black) AABP, (red) p(BP), and (blue) p(BP-b-VP).

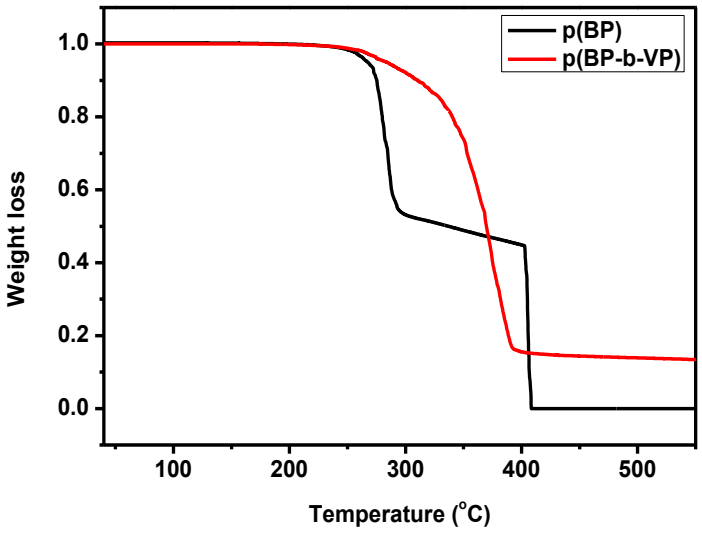

Figure 3. TGA traces for (black) p(BP), and (red) p(BP-b-VP) under a nitrogen atmosphere.

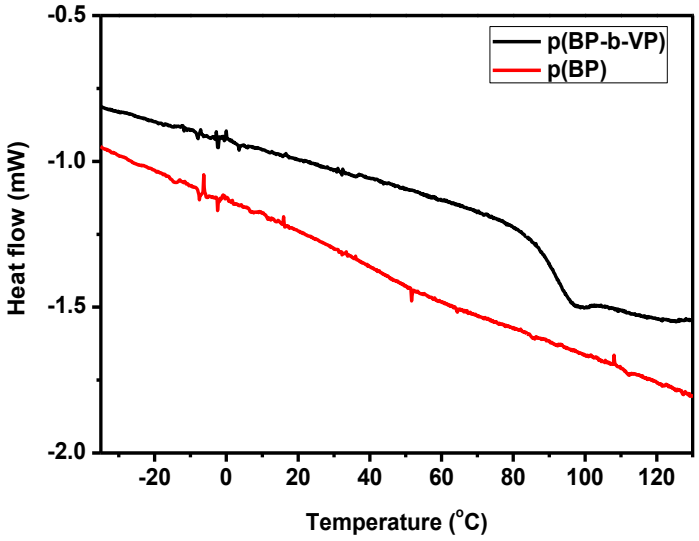

Figure 4. DSC traces for (red) p(BP), and (black) p(BP-b-VP) under a nitrogen atmosphere.

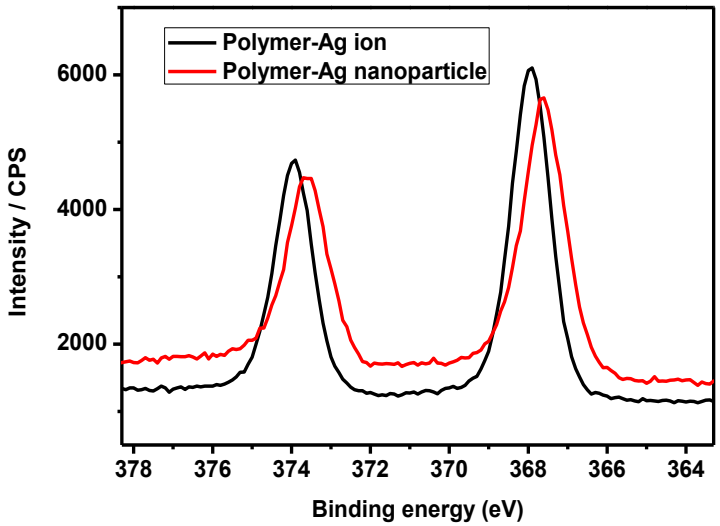

Figure 5. XPS spectra in the Ag 3d region for (black) p(BP-b-VP)-Ag^{+} and (red) p(BP-b-VP)-Ag^{0}.

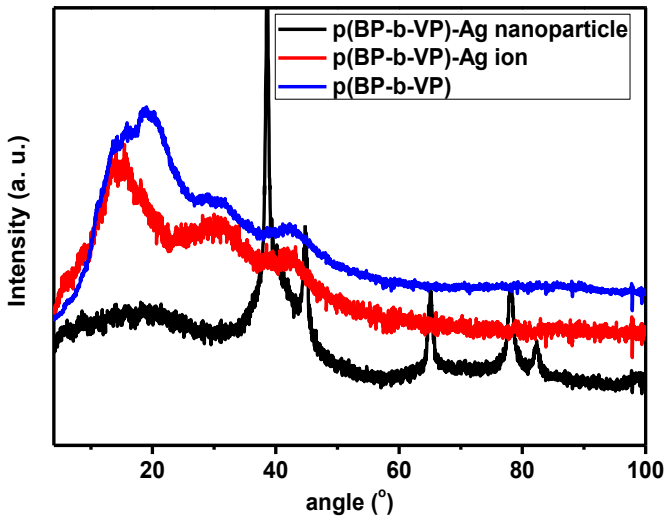

Figure 6. XRD for (blue) p(BP-b-VP), (red) p(BP-b-VP)-Ag^{+} and (black) p(BP-b-VP)-Ag^{0}.

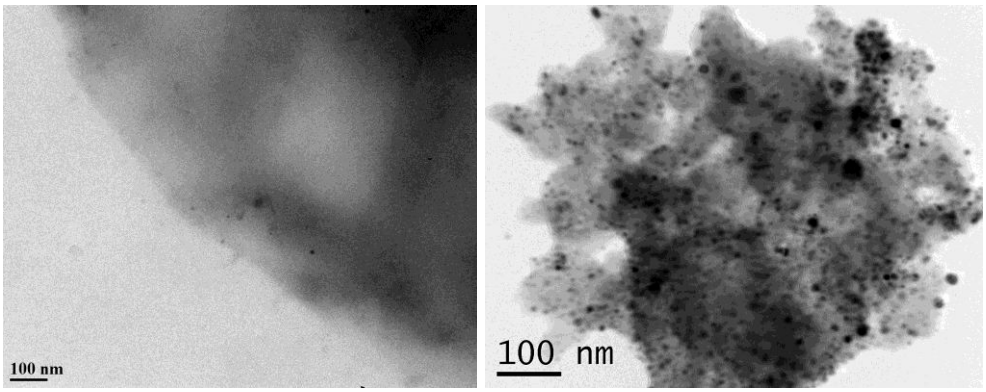

Figure 7. TEM micrographs for (left) p(BP-b-VP)-Ag^{+} and (right) p(BP-b-VP)-Ag^{0}.

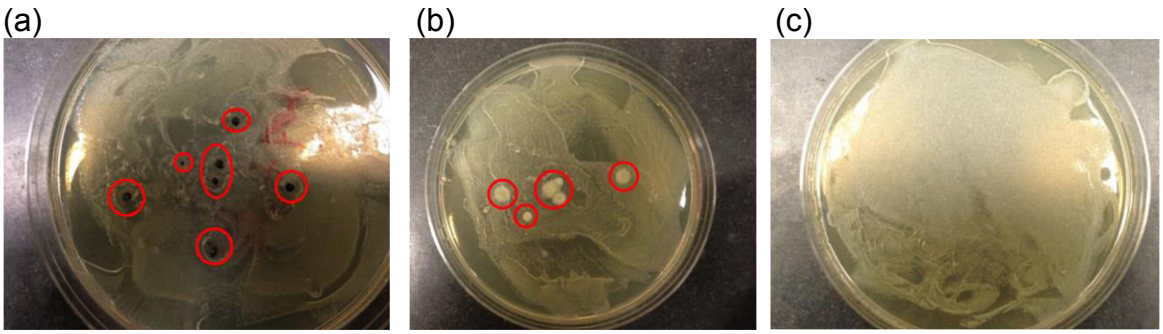

Figure 8. Photographs of agar plates with *L. plantarum* after exposure to (a) p(BP-b-VP)-Ag^0, (b) p(BP-b-VP)-Ag^+, and (c) control experiment.

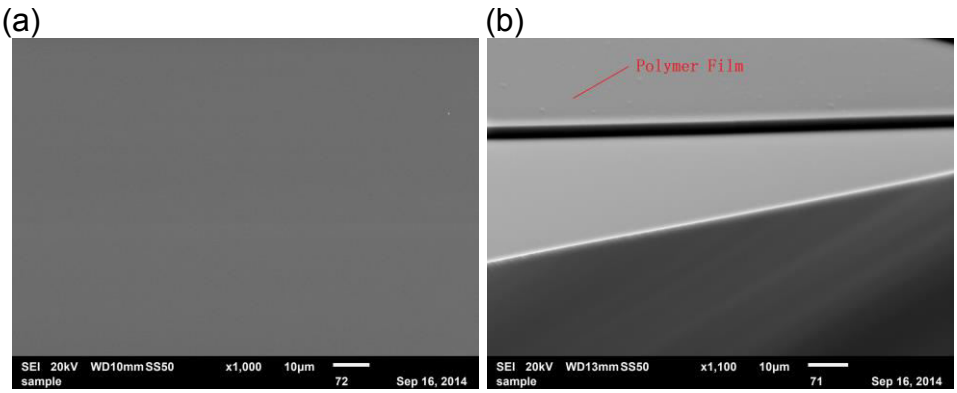

Figure 9. SEM images of p(BP-b-VP) film on glass slides: (a) top surface; (b) cross-section.

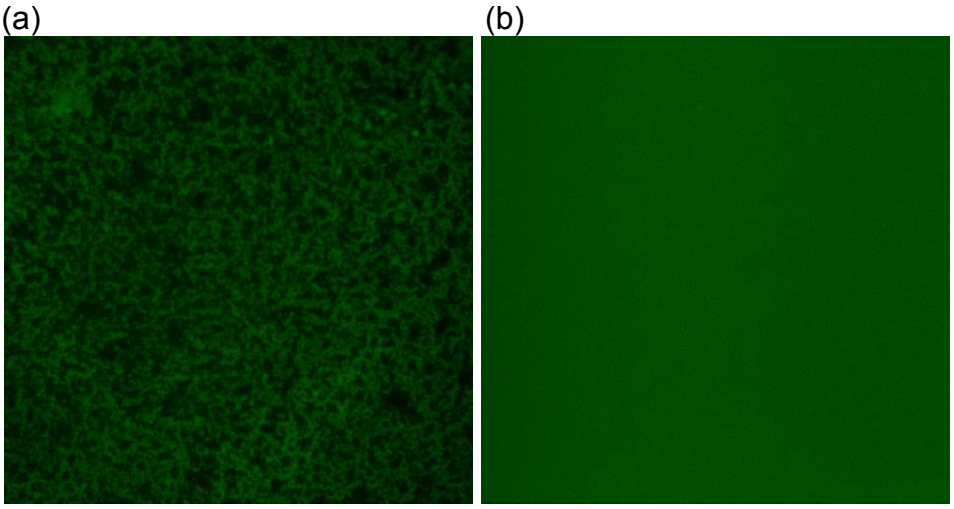

Figure 10. Fuorescence microscope images of fluorescently stained *L. plantarum* attached to glass slide with (a) p(BP-b-VP)-Ag^0 and (b) bare glass after incubation for 20 h.

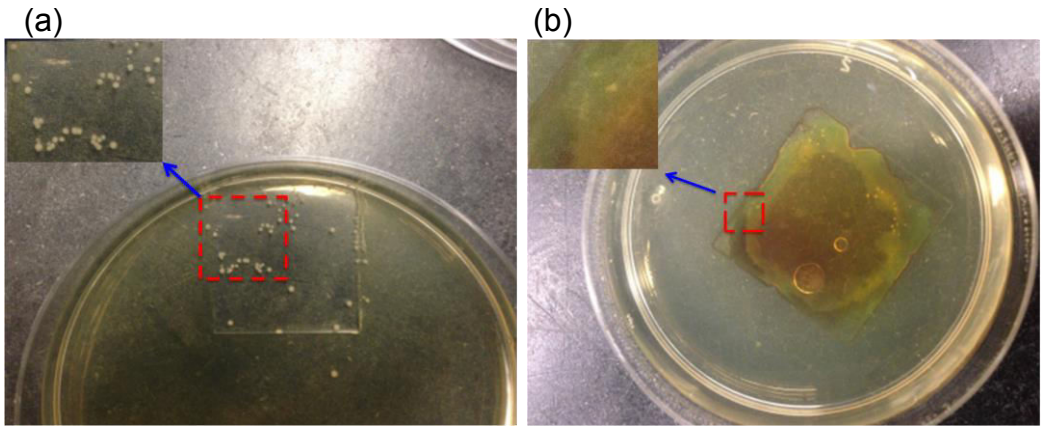

Figure 11. Photographs of (a) blank glass slide, and (b) glass slide coated by p(BP-b-VP)-Ag^0 after 3 days.

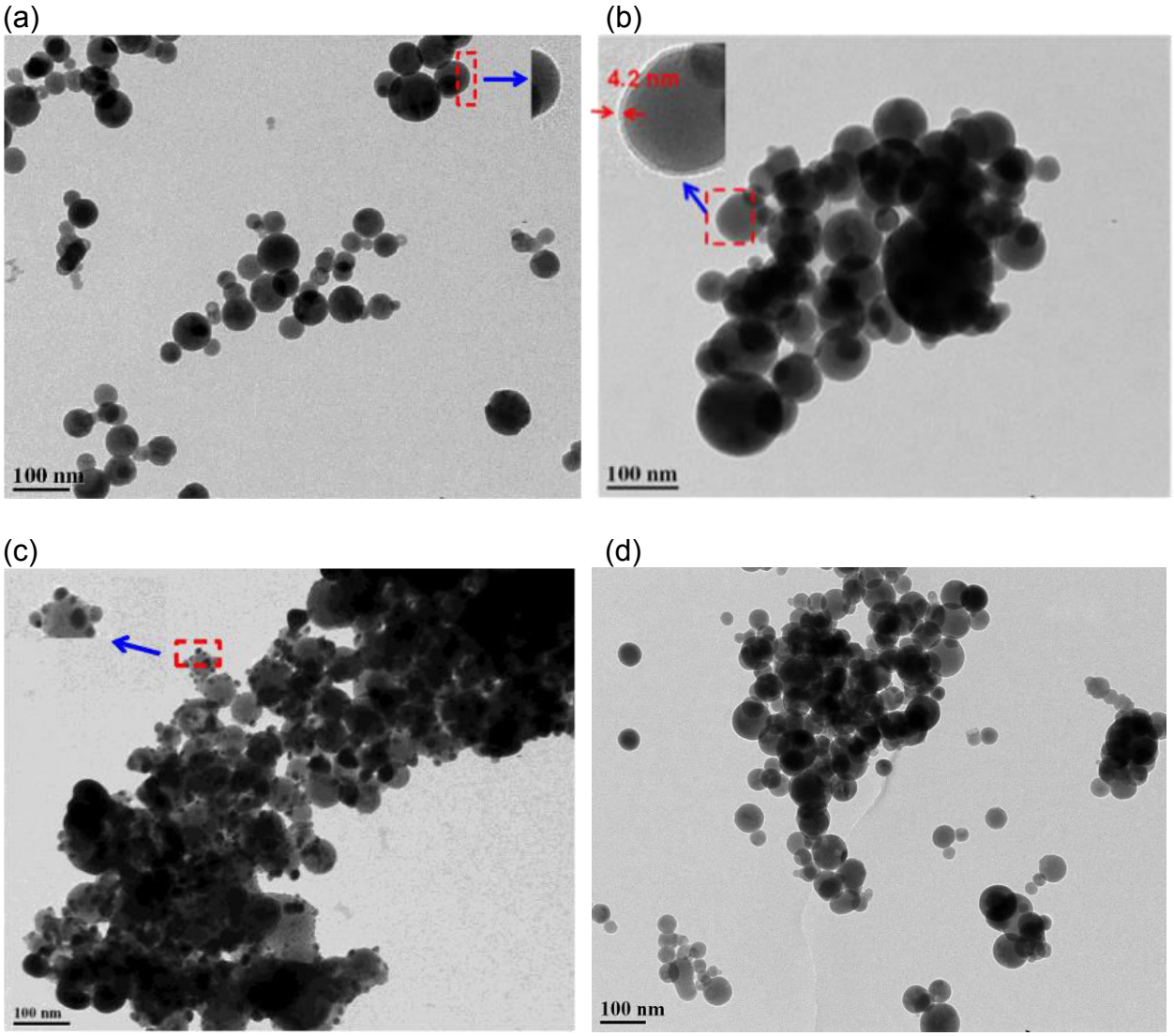

Figure 12. TEM micrographs of (a) HA, (b) HA-p(BP-b-VP), (c) HA-p(BP-b-VP)-Ag^0, and (d) HA-C.

(a) (b) (c)

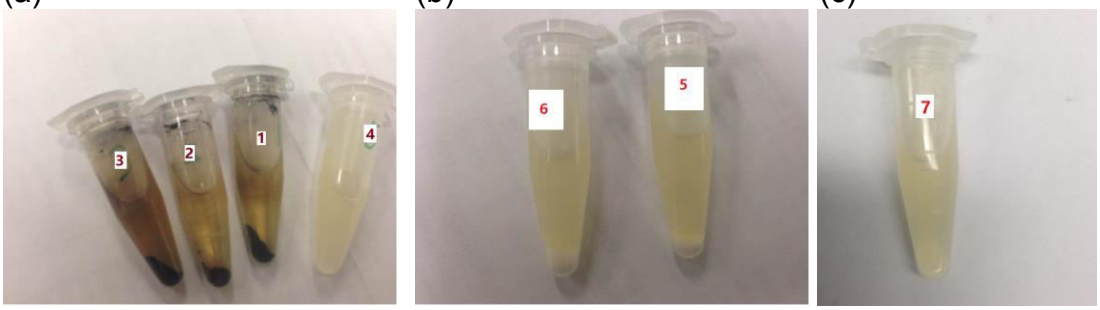

Figure 13. Photographs of (a, 1-3) *L. plantarum* solution treated with HA-p(BP-b-VP)-Ag^0, and (a, 4) a blank, (b, 5,6) *L. plantarum* solution treated with HA, and (c, 7) *L. plantarum* solution treated with HA-C.
Images were aquired after 20 h culture at 37 ^oC.

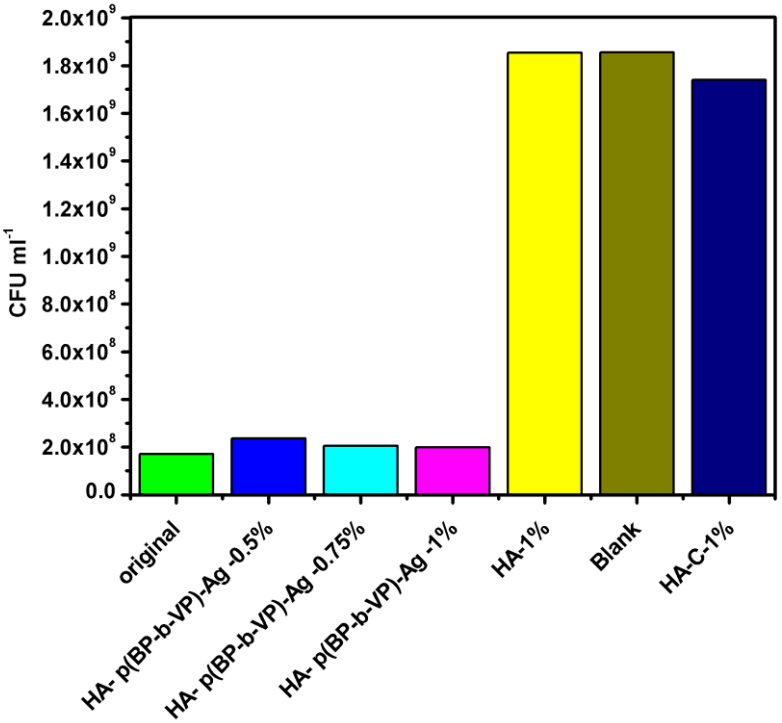

Figure 14. CFUs mL^{-1} of *L. plantarum* after 20 h of growth.

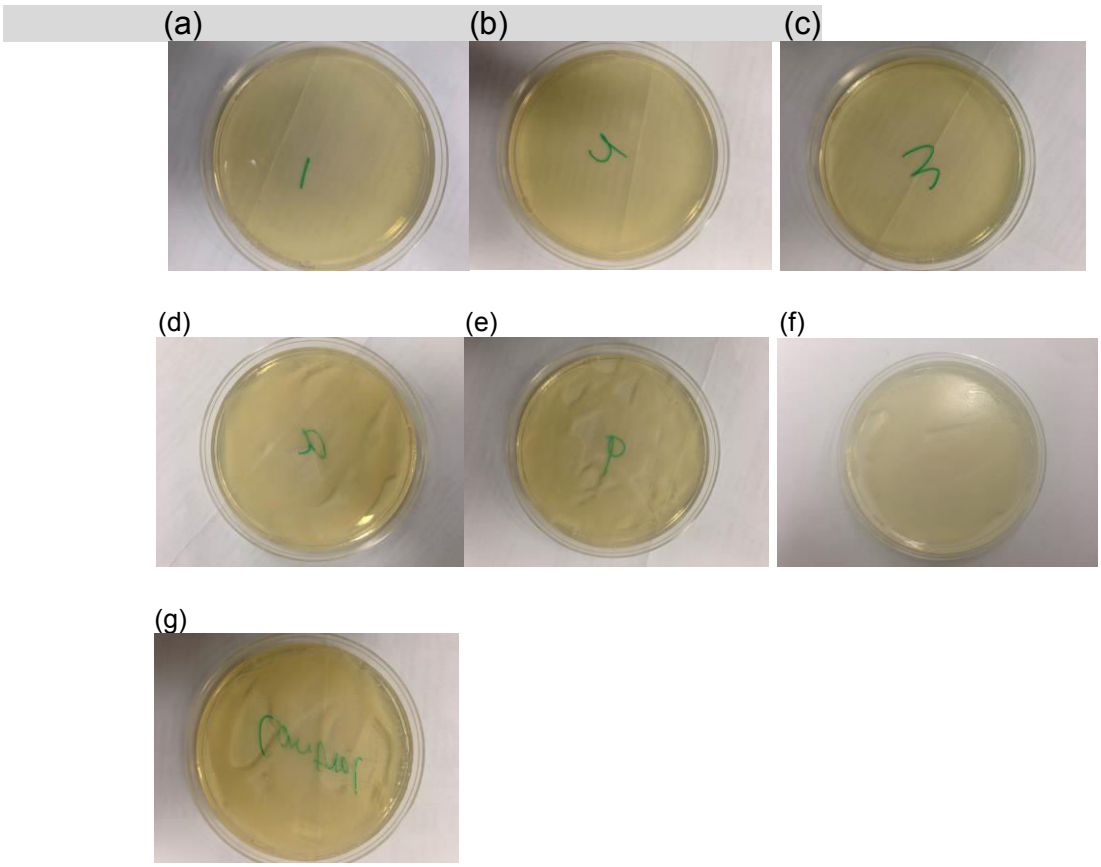

Figure 15. Photographs of samples of *L. plantarum* after exposure to HA-p(BP-b-VP)-Ag^0 (a: 0.5%, b: 0.75%, c: 1%). (d, e): HA (d: 0.5%, e:1 %) treated solution, (f): HA-C (1 %) treated solution and g: blank solution.

TOC